Acta Universitatis Carolinae. Mathematica et Physica

A. Rudajevová; P. Lukáč

Thermal diffusivity and thermal conductivity of $Mg$ alloys and $Mg$-matrix composites

*Acta Universitatis Carolinae. Mathematica et Physica*, Vol. 41 (2000), No. 1, 3--36

Persistent URL: http://dml.cz/dmlcz/142702

# Thermal Diffusivity and Thermal Conductivity of Mg Alloys and Mg-Matrix Composites

A. RUDAJEVOVÁ and P. LUKÁČ

Praha*

*Received 12. October 1999*

The thermal diffusivity and thermal conductivity of Mg, Mg-Sc, AZ91 and QE22 alloys were investigated in the temperature range of 20 to 300°C. The thermal diffusivity and thermal conductivity of Mg-Sc alloys decrease with increasing content of Sc in Mg. The Lorenz number increases with increasing concentration of Sc from $2.52 \times 10^{-8}\,\mathrm{W\Omega K^{-2}}$ for 3.2 wt% Sc up to $3.26 \times 10^{-8}\,\mathrm{W\Omega K^{-2}}$ for 19.09 wt% Sc. The thermal diffusivity and thermal conductivity increase with increasing temperature for all investigated Mg-Sc alloys. The thermal diffusivity and thermal conductivity of AZ91 alloy increase with increasing temperature. The precipitation of $Mg_{17}Al_{12}$ during heating in the first run of the measurement led to an increase in the thermal diffusivity and thermal conductivity. Only small temperature variations of the thermal diffusivity and thermal conductivity were found for QE22 alloy in the temperature range of 20 to 300°C.

The thermal diffusivity and thermal conductivity were investigated for composites: QE22 alloy reinforced by 10, 15 and 25 vol% SiC particles, QE22 alloy reinforced by 20 vol% Saffil fibres and AZ91 alloy reinforced by 22 vol% Saffil fibres. The thermal diffusivity and thermal conductivity of QE22 alloy reinforced by SiC particles decrease with the increasing concentration of SiC particles. The temperature increase of these composites results in a larger decrease of both parameters for the highest temperature and concentration. This is consequence of the interaction of electrons with the lattice imperfections in the interfaces between particles and matrix. The thermal conductivity of the composites was compared with the calculated thermal conductivity using the relation determined by Hasselman and Johnson. The QE22 alloy reinforced by 20 vol% Saffil fibres exhibits

* Department of Metal Physics, Charles University, Ke Karlovu 5, CZ-12116 Praha 2, Czech Republic

a similar behaviour as AZ91 alloy reinforced by 22 vol% Saffil fibres. The anisotropic behaviour was found in the whole temperature range.

## 1. Introduction

In many applications of materials at high temperatures, rates of heat transfer are important. Operating temperatures of mechanical parts, resistance to the thermal stress and others limitations on materials are directly related to the heat conduction and heat transfer. The fundamental equation defining the thermal conductivity in an isotropic solid is:

$$\boldsymbol{q} = -K \, grad \, T \tag{1}$$

where $\boldsymbol{q}$ is a vector of heat flow across the cross-section perpendicular to $\boldsymbol{q}$, $T$ is temperature, $K$ is the thermal conductivity, and the negative sign indicates that heat flow down a temperature gradient from the hotter to the colder regions.

Thermal conduction is the process whereby heat is transferred by interaction between individual atoms, ions or molecules. In the solid, energy is transferred by interaction between neighbouring atoms. There are two processes by which the heat conduction takes place in solids. Heat (energy) can be transferred by coupling between lattice vibrations and/or movement of electrons and collisions with atoms. For a discrete lattice, coupling between normal modes of vibration due to anharmonicities in the lattice vibrations leads to phonon collisions equivalent to random scattering. It is convenient to use a free mean path concept for this process and by analogy with kinetic theory it is possible to write:

$$K_{ph} = \frac{1}{3} c_{ph} v_{ph} l_{ph} \tag{2}$$

where $K_{ph}$ is the phonon thermal conductivity, $c_{ph}$ is the specific heat per volume unit, $v_{ph}$ is the phonon velocity (approximately equal to the sound velocity) and $l_{ph}$ is the phonon mean free path. For the electronic thermal conductivity $K_e$ can be written:

$$K_e = \frac{1}{3} c_e v_e l_e \tag{3}$$

where symbols are the same as in equation. (2).

### 1.1. Factors affecting thermal conductivity of solids

The values of the thermal conductivity of different materials vary over a wide range. Therefore, it is very important to consider the influence of variables before using literature data. The main variables that should be specified are the temperature level, the chemical composition and the arrangement of the different phases which may be present in the material.

a) The temperature dependence of the thermal conductivity

The temperature dependence of the thermal conductivity may be analysed on the basis of Eqs. (2) and (3). In metals the mean free path for the electronic thermal conductivity is proportional to 1/T, specific heat is proportional to T and the electron velocity is nearly temperature independent, so that the electronic contribution does not vary significantly with temperature above room temperature. For pure metals the thermal conductivity decreases with temperature (within available precision of measurements at high temperatures data can be represented by a linear relationship with temperature). A number of high-temperature alloys exhibit an increase in the thermal conductivity with temperature. For crystalline dielectrics, at temperatures above the Debye temperature, the heat capacity is approximately constant, the wave velocity is approximately constant and it was found that the free mean path is proportional to 1/T.

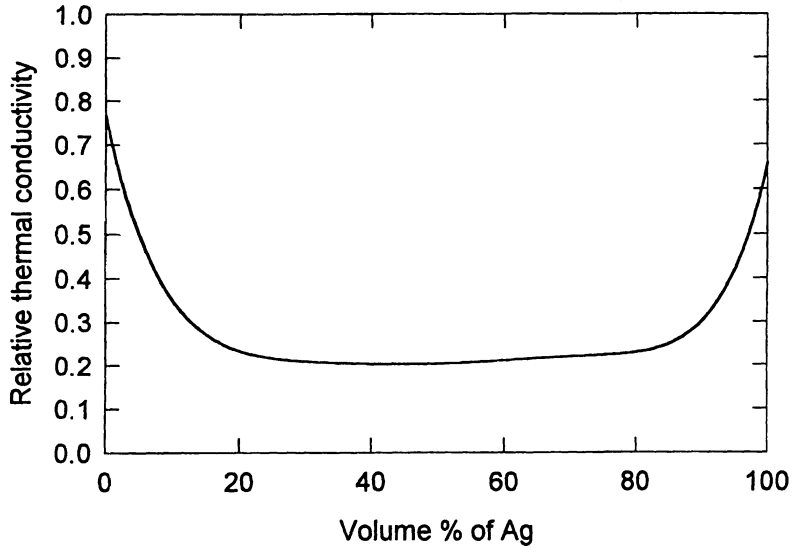


Fig. 1 — Thermal conductivity of Ag-Au solid solution

b) The influence of the chemical composition

Changes in the chemical composition of a single phases have a profound influence on the thermal conductivity, particularly at low temperatures. Impurities in the lattice act as additional disturbances analogous to those of purely thermal origin. The effect of different alloying elements varies markedly. Additions of materials of the same atomic size lead to small differences, whereas additions of materials with quite different atomic size lead to large variations. The thermal conductivity for continuous series of solid solutions shows a minimum at intermediate compositions as shown in Fig. 1 adopted from [1].

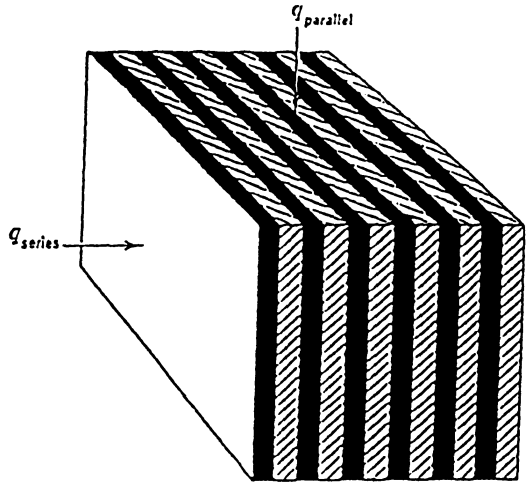


Fig. 2 – Model of the heat flow through the composite slabs

c) The influence of the structure

The structure of a real solid may have as much or more effect as the chemical composition. For a single phase body it has been found that the grain size has no appreciable effect on the thermal conductivity at elevated temperatures primarily because the volume of the grain boundaries is small [2]. However, in materials having anisotropic thermal expansion coefficients, grain boundary cracking may result due to internal stresses and the resultant porosity may have a substantial effect on the thermal conductivity. It is also necessary to consider how critical the arrangement of two phases is on the resultant thermal conductivity. The problem may be approached by considering the composite as shown in Fig. 2 [1]. This composite is formed from slabs of good and poor conductors. If these are arranged parallel to the heat flow ($q_p$ in Fig. 2), they are equivalent to a parallel electrical circuit and the total thermal conductivity is given by the relation:

$$K_t = V_1K_1 + V_2K_2 \tag{4}$$

where $V_1$ and $V_2$ are the volume fraction of each component. In this case, the heat conduction is dominated by the better conductor, and if $K_1 \gg K_2$, then $K_t \cong V_1 . K_1$. On the other hand, if the slabs are arranged normal to heat flow ($q_s$ in Fig. 2), they are equivalent to a series electrical circuit, and the total thermal conductivity is given by relation:

$$K_t = \frac{K_1K_2}{V_1K_2 + V_2K_1} \tag{5}$$

In this case, the heat conduction is dominated by the poorer conductor, and if $K_1 \gg K_2$, then $K_t \cong K_2/V_2$. Although the structures shown in Fig. 2 are extreme

cases, they correspond approximately to structures for which the better conductor is continuous matrix (parallel flow) and for which the poorer conductor is the continuous matrix (series flow). At higher temperatures the effects of chemical composition become less important, but details of the physical structure have an increasing importance.

### 1.2. Measurement of the thermal conductivity

The thermal conductivity may be determined directly by measuring the steady state rate of heat flow per unit area and temperature gradient using relation (1). The thermal conductivity may be determined also indirectly by measurement of the thermal diffusivity under transient conditions. For unidirectional heat flow in a homogenous and isotropic material there is general equation:

$$\frac{dT}{dt} = \frac{K}{Dc}\frac{\partial^2 T}{\partial x^2} \tag{6}$$

The term $K/Dc$ (D is the density and c the specific heat) was first called the thermal diffusivity by Lord Kelvin. Solution of the temperature distributions for a large number of relatively simple shapes and boundary conditions can be found in Ref. [3].

### 1.3. Alloys

In metals and alloys, thermal energy is transported by electrons and by lattice waves. The total thermal conductivity, $K$, of an alloy is usually considered to be the sum of the electronic and lattice (phonon) components of the thermal conductivity:

$$K = K_e + K_{ph} \tag{7}$$

In pure metals, the lattice term is small (very often less than 5 and almost always less than 20%) and the thermal conductivity is dominated by the electronic contribution. The Wiedemann-Franz law relates the electronic part of the thermal conductivity, $K_e$, to the electrical conductivity $\sigma$ at the temperature $T$, through

$$K_e = \sigma \,.\, L \,.\, T \tag{8}$$

where $L$ is the Lorenz number, which under some idealising conditions has the value $L_0 = 2.45 \times 10^{-8}\ \mathrm{W\Omega K^{-2}}$. Often, there is more experimental and theoretical information about $\sigma$ than about $K_e$. In dilute alloys the electrical conductivity is often used for the calculation of the total thermal conductivity (see for example Ref. [4] for Mg alloys). In alloys the impurity scattering of electrons can be so dominant that the electronic thermal conductivity is suppressed enough for the lattice component to represent a considerable contribution. Since this component has no counterpart in electrical conductivity, the thermal conductivity would be underestimated by using the Wiedemann – Franz law and the electrical conductivity for the estimation of $K$.

In most alloys used commercially, the electronic thermal conductivity is depressed; the lattice component is mainly determined by phonon-phonon U-processes and by electron-phonon interactions [5]. The lattice contribution to the total thermal conductivity in alloys can be determined by the relation (7) from the measured total thermal conductivity and the electrical conductivity. This contribution may be determined in alloys more accurately than in pure metals because the lattice contribution to the thermal conductivity in metals is very small.

Magnesium is rarely used for engineering applications without being alloyed with other metals. Key features that dominate the physical metallurgy of the alloys are the hexagonal lattice structure of magnesium c/a = 1.624 and the fact that its atomic diameter (0.320 nm) is such that it enjoys favourable size factors with a diverse range of solute elements. The most widely used magnesium alloy is AZ91 (Mg-9Al-0.7Zn-0.2Mn) in the form of die castings. For applications where greater ductility and fracture toughness are required, a series of high purity alloys with reduced aluminium contents are available. Examples are AM60, AM50 and AM20 alloys (where the concentration of Al is 6, 5 and 2 w%, respectively). The mechanical properties of the AZ and AM series of alloys decrease rapidly with increasing temperature above 120 – 130°C [6, 7]. The most widely used magnesium alloy at elevated temperatures is QE22 (Mg-2.5Ag-2RE(Nd)-0.2Zr). This alloy has been used for a number of aerospace applications including landing wheels, gearbox housing and rotor heads for helicopters [8]. The list of the further magnesium alloys and their applications can be found in the paper of Polmear [9].

### 1.4. Composites

The most published papers concerning Mg alloys and composites are concentrated on investigations of mechanical properties of these materials. Fewer accounts are oriented towards thermal properties. Currently, the area of the thermal conductivity have attracted more attention to expand the applications of composites. The significance of the thermal conductivity for metal-matrix composites (MMCs) in various potential applications has been point out by Kelly [10].

For a heterogeneous materials the effective thermal conductivity (further only thermal conductivity) is defined according to equation (1), where $dT/dx$ is the average value of the temperature gradient over a region that is large in comparison with the size of the heterogeneities. In heterogeneous materials the thermal conductivity depends on:

1) The thermal conductivity of each component
2) The volume fraction of each component
3) The manner in which the components are distributed, in particular:
   a) whether or not one component is continuous in the direction of heat flow
   b) the size, shape and orientation of each segment of each component
4) The nature of the interfaces between the different components.

In metal-matrix composites, there is very often a large difference between the coefficients of the thermal expansion of the ceramic reinforcement and the metallic matrix. Thus any temperature change will lead to the thermal stresses that effect microstructural stability and alter mechanical and thermal properties [11, 12]. For instance, Xu et al. [13] have reported the damage caused by thermal cycling, in terms of elastic modulus and density for magnesium AZ41 alloy reinforced by alumina fibres. The thermal stresses are localised in the vicinity of interfaces that represent discontinuity in the thermal conductivity due to local perturbance of the temperature distribution. Florence and Goodier [14 – 16] considered such thermal stresses near spherical cavities, holes and cracks. Taucher [17] analysed the thermal stresses near a spherical inclusions with thermal and mechanical properties different from those matrix, for the case of perfect thermal contact at matrix-inclusion interface. It was found that the thermal boundary resistance has a significant effect on both the magnitude and the sign of the thermal stresses around reinforcements.

The thermal boundary resistance $R_{bd}$ was originally defined by Kapitza [18] in terms of a temperature drop, $\Delta T$, that occurs across a planar interface between solid and liquid helium, in response to the heat flux, $q$, in a direction normal to the interface:

$$R_{bd} = \frac{\Delta T}{q} \tag{9}$$

In a composite where particles are dispersed in a matrix, a contribution to the thermal conductivity of the composite from interfaces can be more significant than the contribution from the volume of dispersed phase. The effect is stronger for smaller particles because they exhibit a greater surface to volume ratio. The influence of $R_{bd}$ on the composite thermal conductivity was first treated by Hasselman and Johnson [19].

The effective thermal conductivity of a composites may be estimated on the basis of analytic prediction models and determined experimentally. The problem of computing the effective thermal conductivity of heterogeneous mixtures from the thermal conductivities of components is mathematically similar to that for the electrical conductivity, dielectric constant or magnetic permeability of heterogeneous mixture [20, 21]. A solution of the conduction problem requires a knowledge of the shape, size, location and conductivity of each phase of system together with the interaction between particles. Two basic approaches for the calculation of the effective thermal conductivity can be used [22]:

1) Ohm's law models. A basic repeated structural unit representative of the heterogeneous mixture is isolated and equations are derived on the basis of the electrical analogy assuming one-dimensional heat transfer.

2) Fourier's law models. In these models an idealised geometry is assumed (for which the temperature field may be solved). The temperature distribution in the system is determined under assumption a) a regular array of spherical or

b) a random distribution of spherical particles in such small fractions that there is no field interaction. Temperature gradients are then determined and the effective thermal conductivity is established from Fourier-Biot law.

The thermal conductivity of composites is most frequently determined indirectly from the thermal diffusivity. The definition of the thermal diffusivity based on the Eq. (6) supposed an isotropic and homogeneous material. But in general, a composite is not isotropic and homogeneous. This problem was solved for flash method [23] by Kerrisk [24, 25]. In these papers the concept of the thermal diffusivity as a characteristic constant of heterogeneous material was examined and it was found that as long as the dispersed particles are relatively small compared to the total dimension of the sample, the composite appears homogeneous in the transient thermal problem and the equation $a = K/Dc$ can be used.

Magnesium alloys are reinforced by a fairly limited set of reinforcements, specifically SiC and $Al_2O_3$. The SiC particles used in composites and produced from inexpensive raw materials exhibit low density of 3200 kg/m$^3$, low thermal expansion coefficient (TEC) of $4.7 \times 10^{-6}$ K$^{-1}$, and a high Young's modulus of 450 GPa. Commercially available particle sizes range from 1 to 80 μm. The thermal conductivity of SiC is in the range 80 to 200 W/mK depending on purity and processing conditions. For preparation of magnesium-$Al_2O_3$ composites the Saffil fibres (96 – 97% $Al_2O_3$, 4 – 3% $SiO_2$) are used most frequently. The density of this material is 3300 kg/m$^3$, TEC is $7.6 \times 10^{-6}$ K$^{-1}$, Young's modulus is about 380 – 400 GPa and the thermal conductivity at the room temperature is in the range 30 to 36 W/mK. Addition of reinforcements (ceramic particles or fibres) leads to an increase in strength, Young's modulus and hardness. The most used Mg alloys for preparation of composites are alloys AZ91, QE22, AS41 or WE43 (see for example [26 – 31]).

## 2. Experimental part

### 2.1. Preparation of materials

#### 2.1.1. Alloys

The MgSc4 – MgSc16 alloys were produced in the Institut für Werkstoffkunde und Werkstofftechnik, TU Clausthal (IWW). The starting materials were magnesium with a purity of 99.9 wt.% and metallic scandium of 99.99 wt.%. The procedure adopted was to stir the scandium into the magnesium melt. The alloys designated as MEL was produced at Magnesium Electron LTd., Manchester, UK. The composition of alloys is given in Table 1.

#### 2.1.2. Composites

The powder metallurgical production of the QE22/SiC MMC was carried out by hot extrusion after mixing and milling of QE22 matrix powder ($d_{50}$ = 39 μm) and

SiC particles ($d_{50}$ = 9 μm). The powder/particle blends were precompacted and encapsulated. The capsules were heated up to 400°C before extrusion, which was executed to a degree of deformation between $\ln(S/S_0)$ = 2.8 and 3.0. The particles became aligned parallel to the direction of extrusion showing a uniform distribution in the cross section of the extruded rods. The specimens were investigated in the as extruded state.

**Table 1** – Composition of MgSc alloys

| Alloy Designation | Nominal Sc content [wt.%] | Actual Sc content [wt.%] | Casting Route |
|---|---|---|---|
| MgSc4 | 4 | 3.23 | squezze-casting |
| MgSc8 | 8 | 7.42 | squeeze-casting |
| MgSc12 | 12 | 10.14 | squeeze-casting |
| MgSc16 | 16 | 11.11 | squeeze-casting |
| MgSc12MEL | 12 | 14.54 | sand casting |
| MgSc16MEL | 16 | 19.09 | ingot casting |

Reinforced QE22/20 vol% Saffil and unreinforced specimens of the QE22 alloy were produced by squeeze casting. The procedure is based on forcing (in two steps at 50 and 130 MPa, respectively) the melt (approximately 800°C) into a fibre preform (approximately 1000°C). The preform consist of approximately 20 vol% planar isotropically distributed δ-alumina short fibres (Saffil RF grade from ICI, 96 to 97% $Al_2O_3$, 4 to 3% $SiO_2$, 3 μm in diameter with the mean length of about 87 μm according to SEM estimations after squeeze casting). An alumina binder ensures easy handling of the preform and dimensional stability during casting. Preheating of the preform to a temperature higher than the melt temperature avoids the beginning of the solidification at the fibre during the melt infiltration. The squeeze casting technology guarantees the short time of contact between the liquid metal and the fibres. Consequently only a slight reaction between the fibres and the matrix is observed resulting in occasional reaction products and precipitates. The as-cast specimens show α-Mg solid solution with large precipitates containing Ag, Nd and O and the intermetallic compound $Al_2Nd$ preferentially situated at the fibres or the grain boundaries. $Mg_2Si$ and $Mg_{17}Al_{22}$ particles were found at the matrix-fibre interfaces due to reactions of the melt with the Saffil fibre and/or the inorganic binder. All materials prepared were exposed to the T4 heat treatment, i.e. solution annealing 520°C/5.5h followed by hot water (70 to 90°C) quench.

Reinforced and unreinforced specimens of the AZ91 alloy were produced simultaneously by squeeze casting. The final fibre volume fraction after squeeze casting was about 22 vol% of Saffil. $Mg_2Si$ and $Mg_{17}Al_{12}$ particles were found at the matrix-fibre interfaces due to reactions of the melt with the Saffil fibre and/or

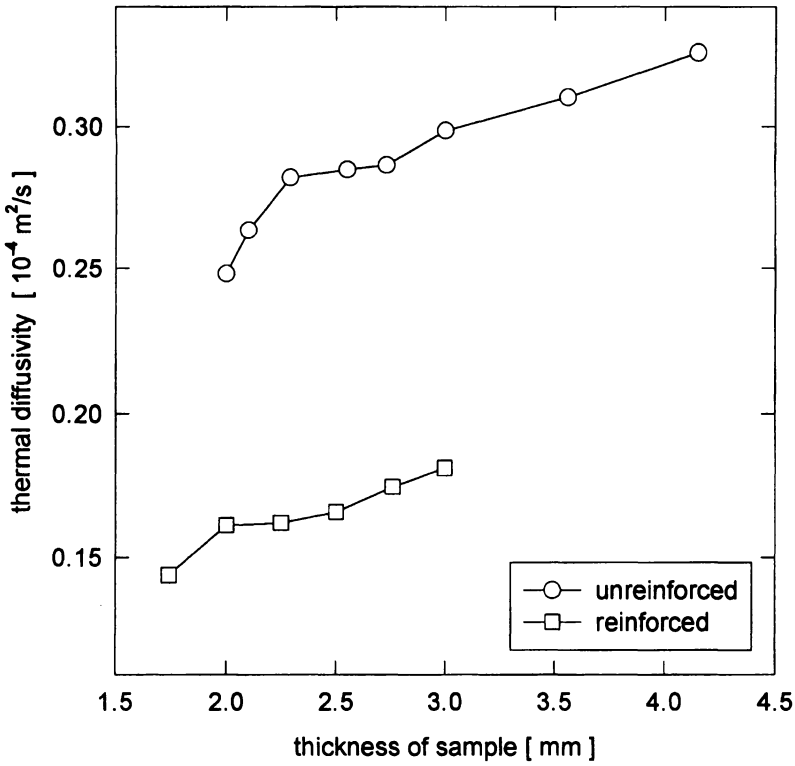


Fig. 3 – Dependence of the thermal diffusivity on the sample thickness of Saffil fibre reinforced and unreinforced AZ91 alloy. Thermal diffusivity was measured at 20°C

the binder between the fibres. The materials were exposed to the T4 heat tratment, i.e. solution annealing 413°C/18h finished by air cooling.

### 2.2. Determination of the thermal conductivity

The thermal conductivity was estimated from the relation $K = aDc$, where the thermal diffusivity and the density were measured and $c$ was calculated. The specific heat of unreinforced alloy was calculated by the Neumann – Kopp rule, the specific heat of composites by the equation:

$$c_c = \frac{f_m D_m c_m + f_d D_d c_d}{D_c} \tag{10}$$

where $f$ is the volume fraction, $c$ is the specific heat per mass unity, $D$ is the density and subscripts $c$, $m$ and $d$ denote the composites, matrix and dispersed particulate, respectively. The temperature dependence of the density was determined by the relation:

$$D = D_o\left(1 + \frac{\Delta l}{l_0}\right)^{-3} \tag{11}$$

where $D_o$ is the density of the material at room temperature and $\Delta l/l_0$ is the relative elongation of the material. The temperature dependence of the relative elongation was measured in argon atmosphere using Netzsch dilatometer. The rate of heating was 5 K/min.

The measurement of the thermal diffusivity was carried out in the temperature range of 20°C to 300°C in an argon atmosphere using the flash method. Flash methods are those, whatever the geometry of the sample, in which a flash of thermal energy is supplied to a sample surface within a time interval that is short compared to the time required for the thermal pulse to propagate through a thin sample. Experimentally, they are characterised by their great simplicity, by requiring only small amounts of material, and by being readily extended to high temperatures. Freedom from heat-loss problem stems largely from the short-time aspect of the method. Parker et al. [23] were the first who used flash method to measure the thermal diffusivity over a wide range of temperature. Their results

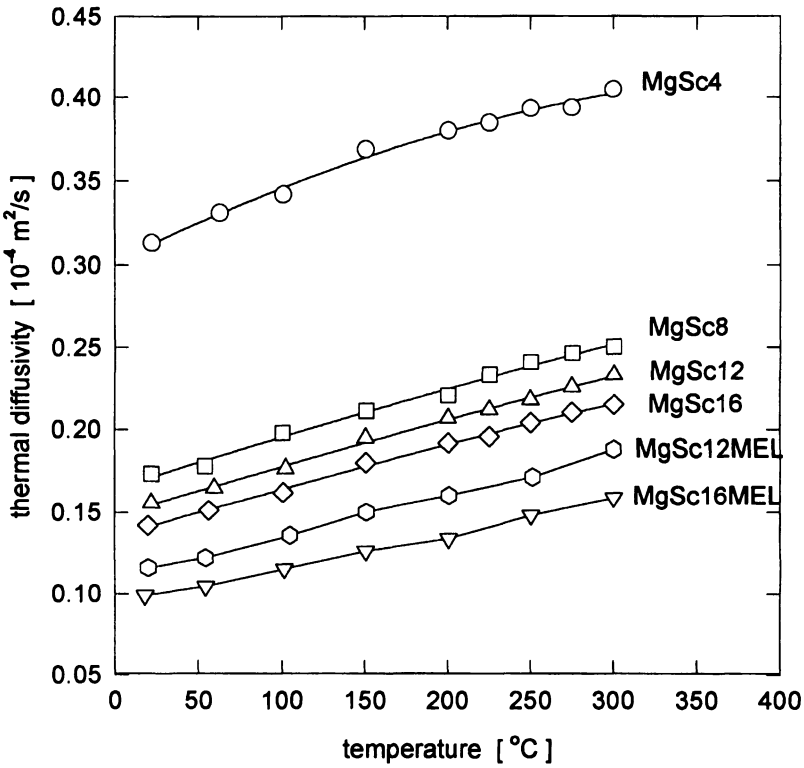


Fig. 4 — Temperature dependence of the thermal diffusivity of Mg-Sc alloys

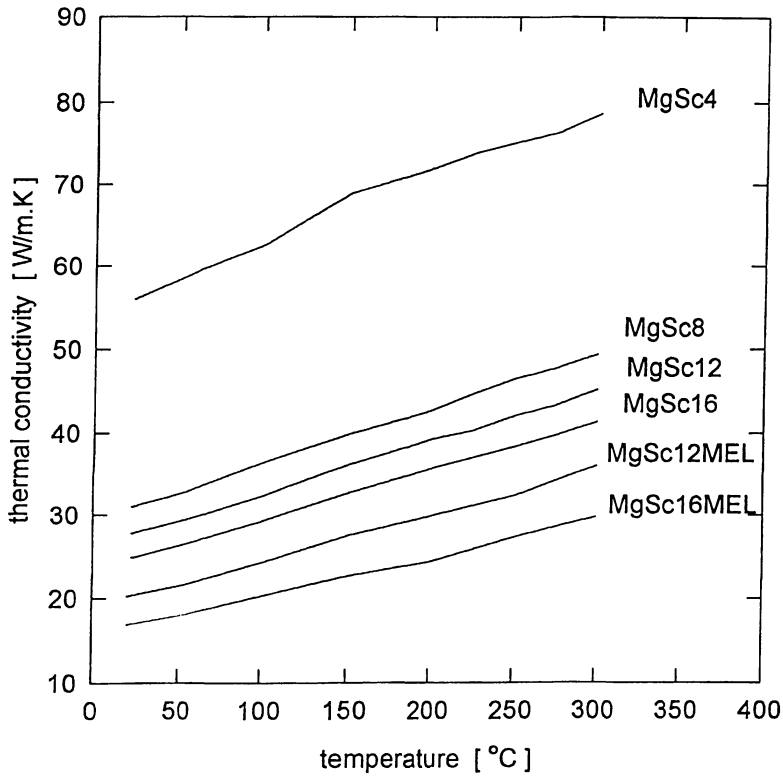


Fig. 5 — Temperature dependence of the thermal conductivity of Mg-Sc alloys

demonstrated that the method yielded data that were in excellent agreement with those obtained by other methods. The flash method is applicable to materials with a wide range of the thermal diffusivities. The source of radiant energy is usually a xenon flash lamp or a laser. After irradiation of a surface of the specimen the resultant temperature excursions at the rear face of the specimen are recorded and the thermal diffusivity is computed from the resultant temperature rise versus time data. Transient times are usually less than 1 s. The thermal diffusivity is calculated using the relation:

$$a = \frac{0.1388 \cdot l^2}{t_{1/2}} \tag{12}$$

where $l$ is the specimen thickness and $t_{1/2}$ is the elapsed time needed for the rear face temperature to reach one-half of its maximum rise. In this method there is defined the characteristic time $t_c$ as

$$t_c = \left(\frac{l}{\pi}\right)^2 \left(\frac{1}{a}\right) \tag{13}$$

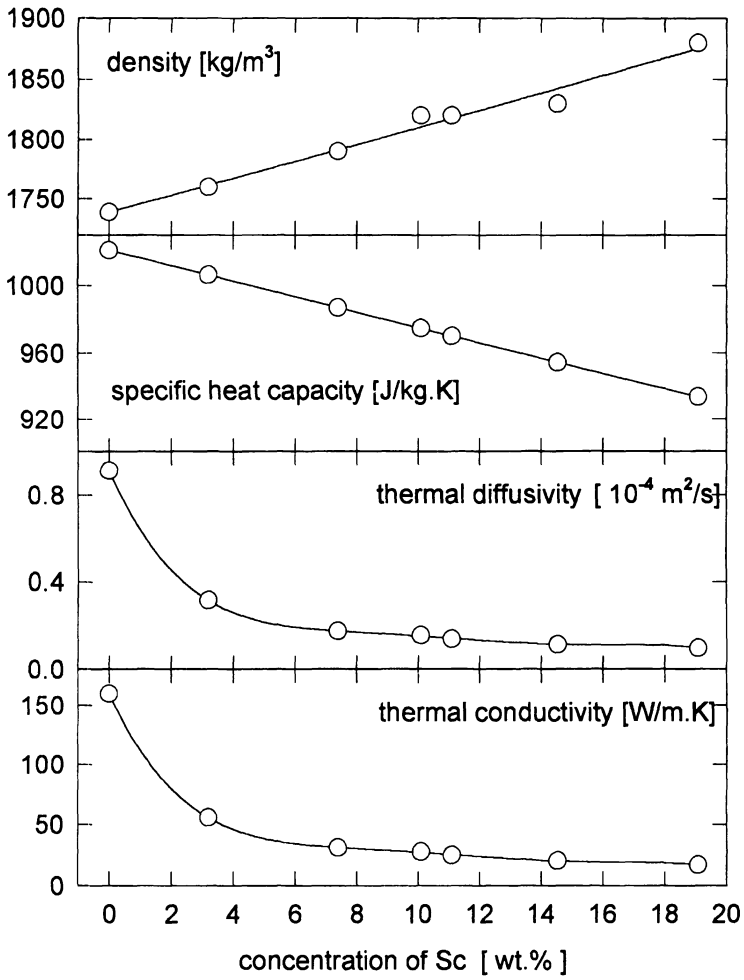


Fig. 6 — Thermal properties of the Mg-Sc alloys at room temperature

It is important that the duration of the radiation pulse incident on the front face of the specimen be negligble compared with the characteristic time [32].

The thermal diffusivity of a metal is generally considered to be independent of its thickness. During the measurement of the thermal diffusivity by the flash method it was, however, found that there is so-called "thickness effect". The origin of this effect may be a consequence of more than one phenomenon [33]. It was found that the thermal diffusivity increases with increasing sample thickness [34].

The thermal diffusivity in our specimens were measured in an argon atmosphere, using the apparatus described elsewhere [35]. The source of the light flash was Xe tube, with a pulse duration of 1 ms. The resultant temperature rise at the rear face

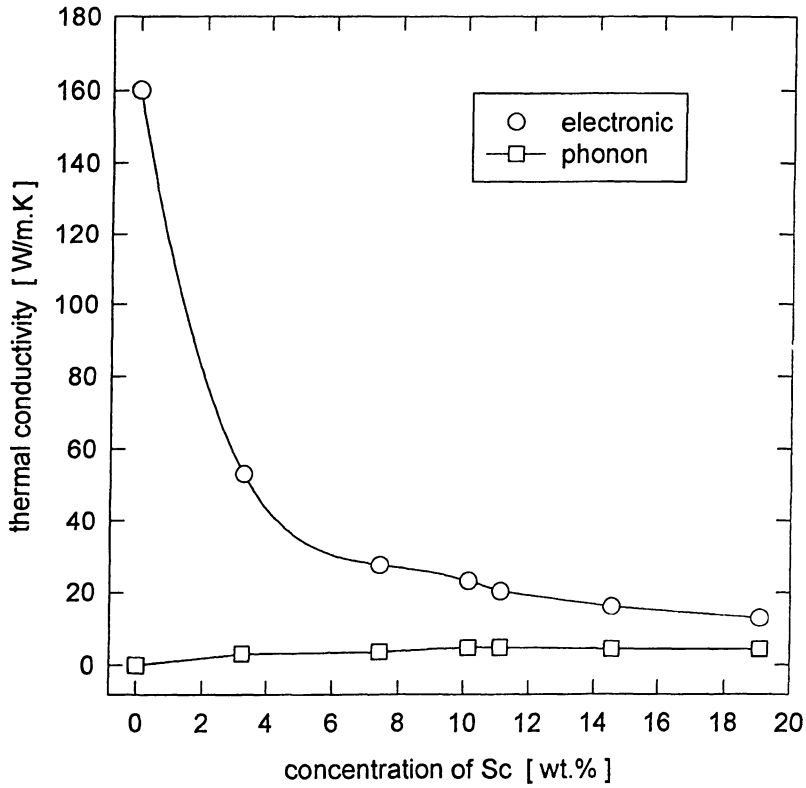


Fig. 7 – Concentration dependence of the electronic and phonon thermal conductivity at room temperature

of the specimen was about 1°C. The measurement of each point for the temperature dependence was started after holding the specimen 10 minutes at the temperature of the measurement.

## 3. Result and Discussion

### 3.1. Alloys

The thickness dependence of the thermal diffusivity for AZ91 alloy and composite AZ91/22 vol.% Saffil is shown in Fig. 3 [36]. The optimum specimen thickness was settled by the minimal slope of the curves in Fig. 3. The optimum specimen thickness of 2.5 mm and 2.1 mm was determined for reinforced and unreinforced AZ91, respectively. These thicknesses of specimens were chosen for further experiments. They indicated a characteristic time $t_c = 0.023$ s for unreinforced and $t_c = 0.029$ s for reinforced AZ91 alloy, respectively. Both characteristic times are much larger than the duration of the heat pulse (0.001 s). The

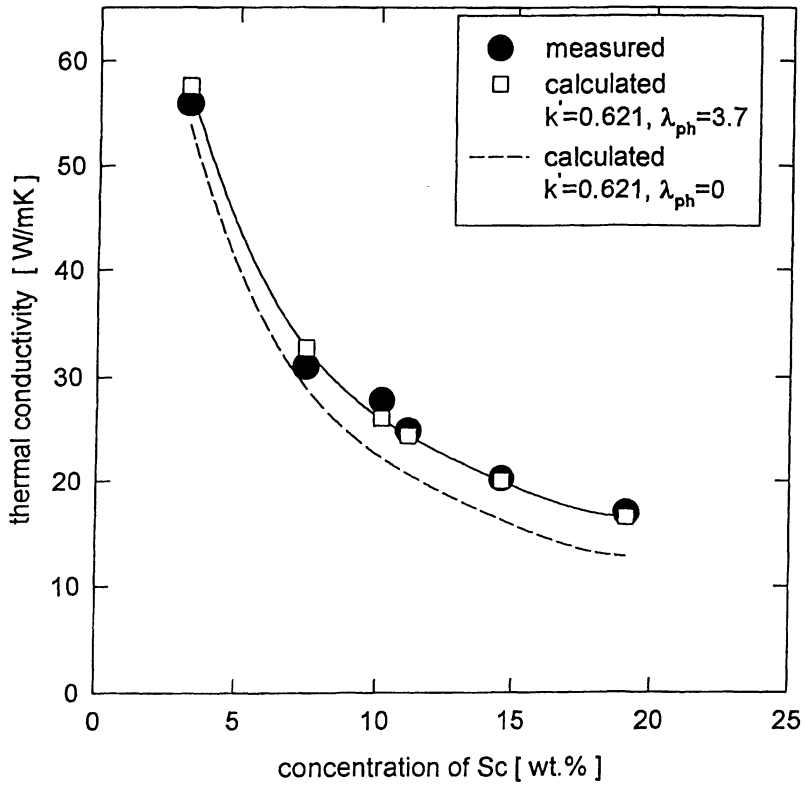


Fig. 8 — Concentration dependence of the calculated and measured thermal conductivity at room temperature for Mg-Sc alloys

thickness of the other materials investigated in this work was in the range of 2 to 2.5 mm.

The new magnesium alloys based on the Mg-Sc system are interesting for the following reasons:

1) alloying with scandium enhances the melting point of Mg-Sc solid solutions,
2) the high melting point of Sc (1541°C) compared with other rare earth metals implies a lower diffusivity in Mg,
3) the density of Sc (3000 kg/m$^3$) is lower than that of comparable alloying elements.

Owing to good creep resistance, these alloys, particularly after alloying with further elements as Al, Y, Nd, Ga, La, Ce or Mn, are potencial candidates for using at elevated temperatures.

Figure 4 shows the temperature dependence of the thermal diffusivity for all the Mg-Sc alloys under investigation. In the figure only the values for the first run are shown for each alloy. Two specimens were produced of each composition and two runs were made of each specimen. The maximum difference between single

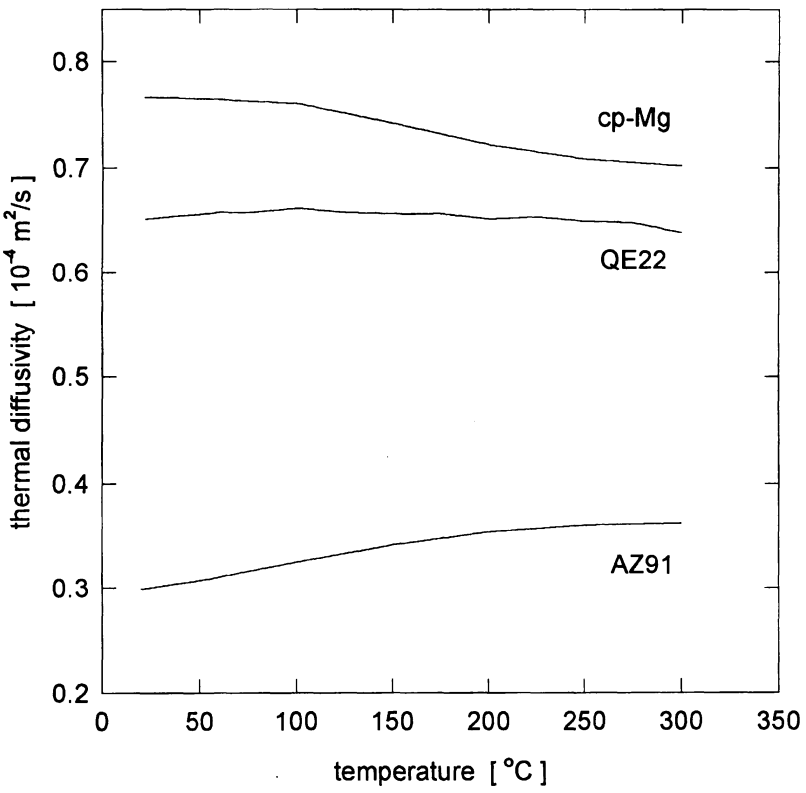


Fig. 9 — Temperature dependence of the thermal diffusivity of cp-Mg, QE22 and AZ91 alloys

measurements was about 10%. The temperature dependence of the thermal conductivity is shown in Fig. 5. Each curve in Fig. 5 is the average of four measurements. Both the thermal diffusivity and the thermal conductivity increase with increasing temperature and decrease with increasing Sc content. The density, specific heat, thermal diffusivity and thermal conductivity of the various Mg-Sc alloys at room temperature are shown in Fig. 6 as a function of the Sc content. Only the density increases with the Sc concentration whereas the specific heat, thermal diffusivity and thermal conductivity decrease with increasing content of Sc in the alloys.

The composition dependence of electrical resistivity for binary alloys was characterised by Nordheim and the following relation known as Nordheim's law [37] can be used:

$$\varrho = (1 - x)\,\varrho_A + x\varrho_B + kx(1 - x) \tag{14}$$

where $\varrho_A$ and $\varrho_B$ is the electrical resistivity of the pure elements $A$ and $B$ respectively, $x$ is the atomic fraction of the element $B$ and $k$ is a positive constant that

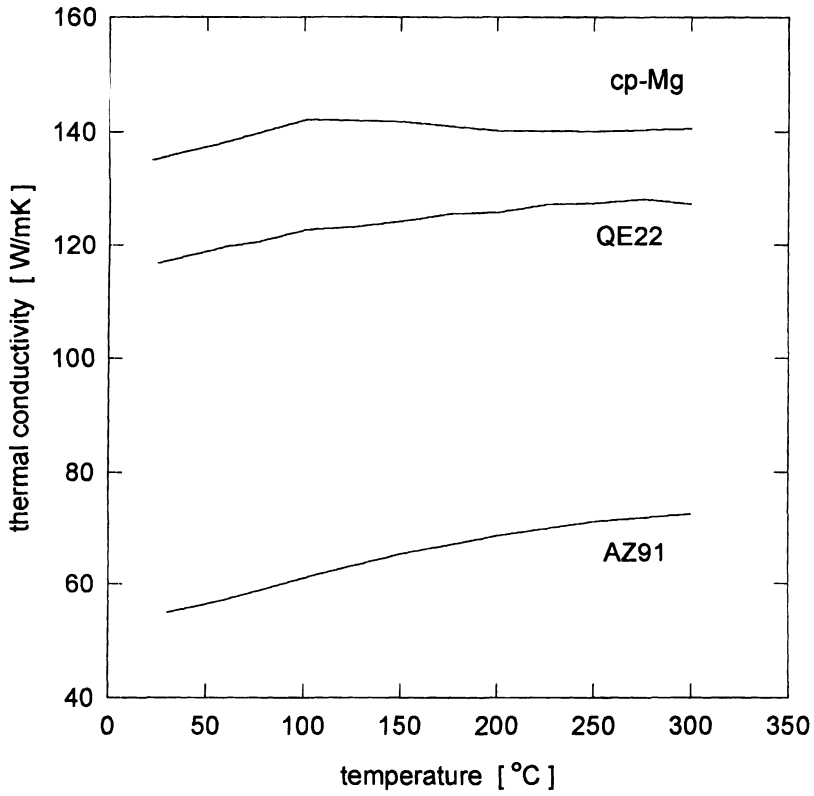


Fig. 10 – Temperature dependence of the thermal conductivity of cp-Mg, QE22 and AZ91 alloys

depends on the alloy system. Providing that the Lorenz numbers do not change considerably for both components and solid solutions, the Nordheim's law can be readily converted to the analogous relation for the electronic thermal conductivity $K_e$ using the Wiedemann–Franz law in which the electronic thermal conductivity is inversely proportional to the electrical resistivity as follows [38]:

$$K_{ss} = \frac{1}{\frac{1-x}{K_A} + \frac{x}{K_B} + k'x(1-x)} \qquad (15)$$

where $K_A$ and $K_B$ are the electronic thermal conductivities of the elements $A$ and $B$ and $k' = k/L_oT$. The Lorenz numbers are given in Tab. 2. It is important to note that the relation (15) is based only on the electronic thermal conductivity. According to equation (7) the thermal conductivity of alloys is given as a sum of the electronic and the phonon thermal conductivity. The electronic thermal conductivity was calculated using Wiedermann–Franz law with the Lorenz number $L_o = 2.45 \times 10^{-8}\ \mathrm{W\Omega K^{-2}}$ and the electrical resistivity data from [39]. The

**Table 2** — The Lorenz numbers

| concentration of Sc [wt.%] | $L \times 10^8$ [$W\Omega K^{-2}$] |
|---|---|
| 0 | 2.47 |
| 3.23 | 2.52 |
| 7.42 | 2.69 |
| 10.14 | 2.87 |
| 11.11 | 2.95 |
| 14.54 | 2.98 |
| 19.09 | 3.26 |

phonon thermal conductivity was calculated from the relation (7) as the difference between the total thermal conductivity and the electronic thermal conductivity. The concentration dependence of the electronic and phonon thermal conductivity is shown in Fig. 7. It can be seen that while the phonon thermal conductivity is nearly constant, the electronic thermal conductivity decreases with increasing Sc content.

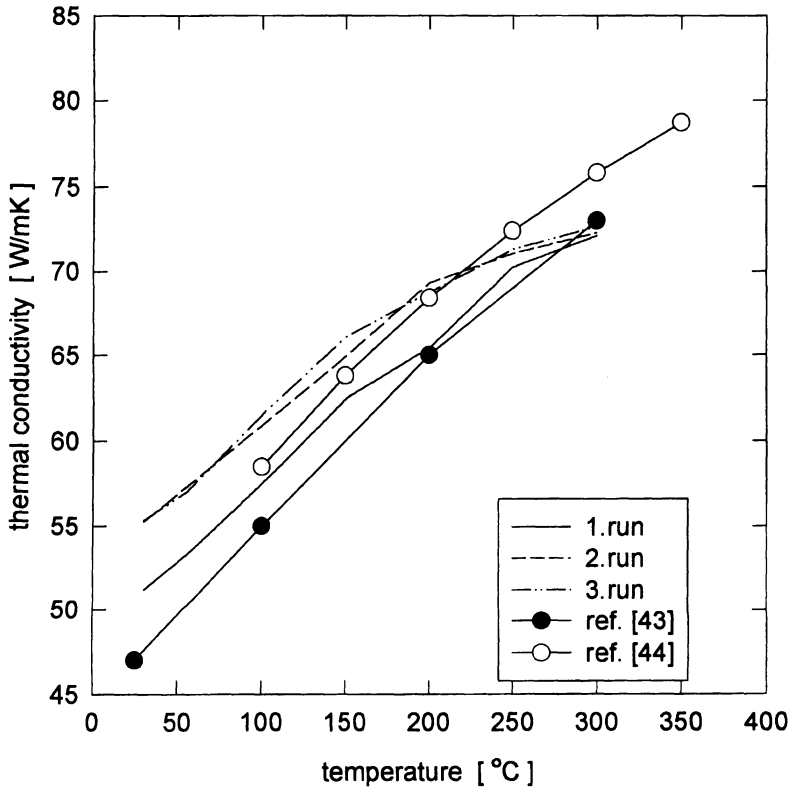


Fig. 11 — Temperature dependence of the thermal conductivity of AZ91 alloy

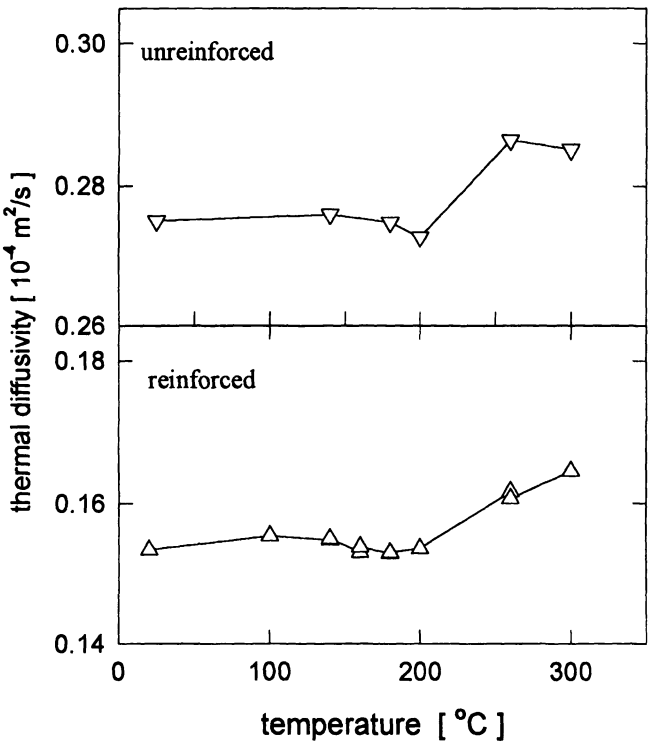


Fig. 12 – Dependence of the thermal diffusivity on the precipitation process (isochronally annealed up to various upper temperatures)

The impurity scattering of electrons increases with increasing Sc content so that the electronic thermal conductivity is suppressed sufficiently and the phonon component represents a considerable contribution at the highest Sc concentration. The phonon contribution to the thermal conductivity should be taken into account in the calculation of the thermal conductivity. Using equations (14) and (15) a good agreement of calculated and measured data is obtained only for $K_{ph} = 3.7$ W/mK. It is the full line in Fig. 8. The dashed line represents calculated data for $K_{ph} = 0$. In this case a rather a poor agreement between the measured and calculated values is obtained. We are aware that for a real system Mg-Sc with the varying Sc concentration the electronic part of the thermal conductivity can be considerably effected due to a change of electronic structure and scattering potential upon alloying the Mg with Sc. The effect of alloying is respected in the Nordheim's relation in the third term of the equation (14) $kx(1 - x)$, where $k$ is a constant. In the equation (15) the effect of alloying on the electronic thermal conductivity is expressed in the term $k'x(1 - x)$, where $k' = k/L_oT$. When the change of the electronic structure is respected in alloying term of both equations, the shift of the dashed curve in Fig. 8 may be ascribed to the phonon contribution by the relation

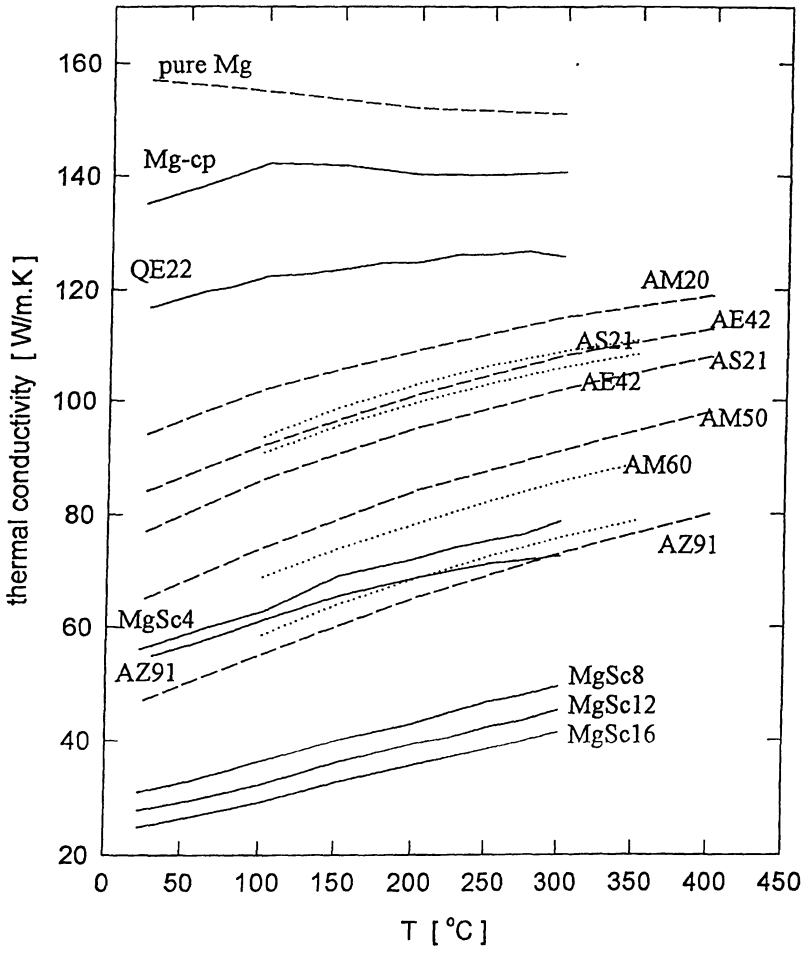


Fig. 13 – Temperature dependence of the thermal conductivity of Mg alloys; full lines- measured here, dotted lines [44], dashed lines [43]

(4). From this analysis it can be seen the error caused by replacing of the total thermal conductivity by the electronic thermal conductivity. The smallest error is obtained for the lowest concentration of Sc in alloy (about 7 wt%) and the highest one for the largest concentration of Sc (about 19 wt%).

The most industrial used Mg alloys are AZ91 and QE22 alloys. The temperature dependencies of the thermal diffusivity of these alloys are shown in Fig. 9. In the figure the temperature dependence of the thermal diffusivity of cp-Mg (commercial purity; Mg-0.6wt%Al-0.2wt%Si) is presented, too. The temperature dependence of the thermal conductivity of these alloys is given in Fig. 10. It can be seen that the largest value of the thermal conductivity is for the alloy with the lowest amount of alloying elements. The thermal conductivity of cp-Mg has a character of alloy

up to 100°C, e.i. it increases with temperature. Above 100°C it decreases with temperature as in the case of a pure metal.

The thermal diffusivity and thermal conductivity of AZ91 were determined for 3 runs up to 300°C. From Fig. 11 it can be seen that the thermal conductivity for 2. and 3. run is the same and it is larger than for 1. run. The differences in both the thermal diffusivity and the thermal conductivity between the first and further runs are due to the precipitation process that is connected with the purification of alloy. According to data in the literature [40–42] the decomposition sequence of a supersaturated solid solution of Al in the AZ91 alloy is very simple, involving only the formation of incoherent particles of the equilibrium β-phase ($Mg_{17}Al_{12}$) without any formation of Guinier-Preston zones or intermediate precipitates. The dependence of the thermal diffusivity on the precipitation process in the alloy (isochronally annealed up to various upper temperatures) is shown in Fig. 12. A significant increase in the thermal diffusivity for isochronal annealing temperatures above 200°C is caused by the removal of solute from the alloy due to precipitation of the β-phase.

Two dependencies given in the literature [43, 44] are also shown in Fig. 11. Kaschnitz and Funk [44] measured the thermal conductivity by steady state method using the Dynatech comparative instrument. The thermal conductivity data in [43]

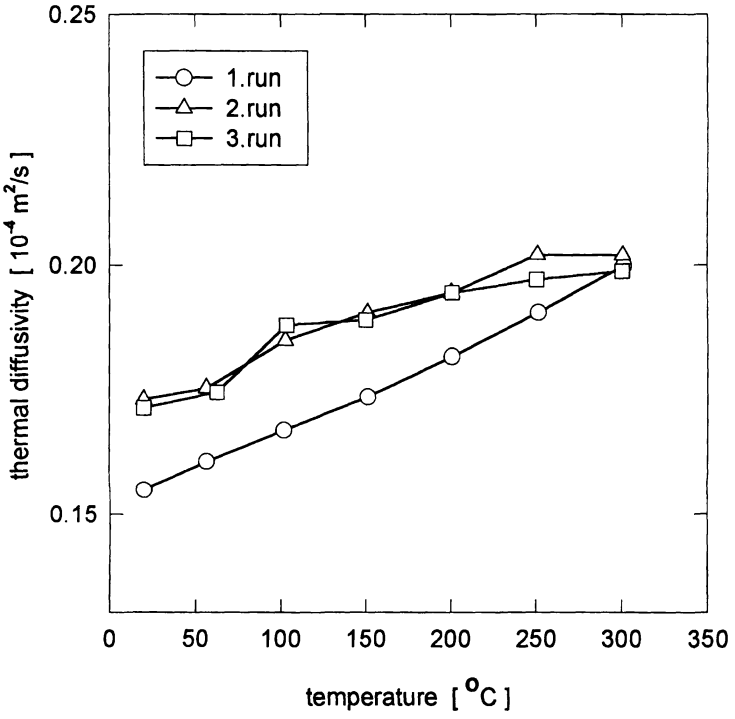


Fig. 14 – Temperature dependence of the thermal diffusivity of the first, second and third run for AZ91 with 22 vol% Saffil

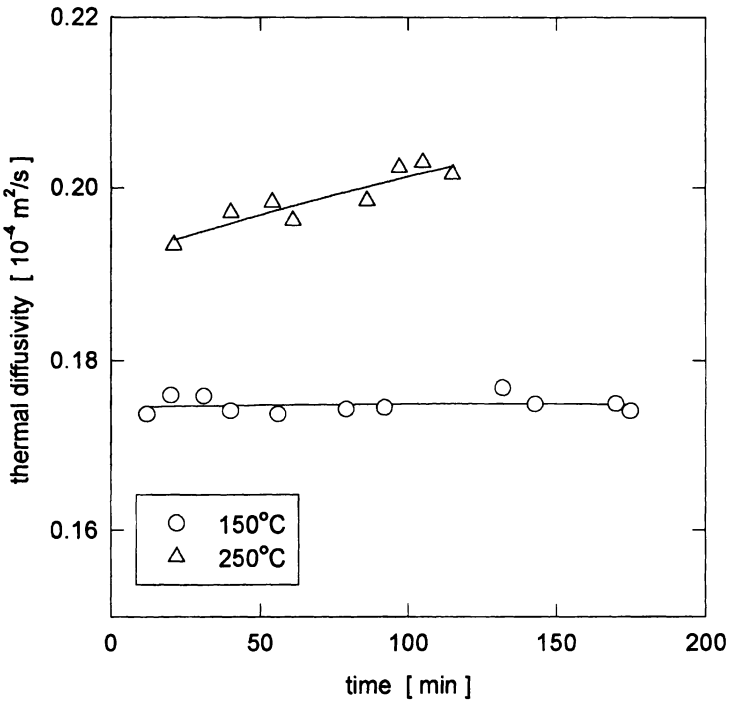


Fig. 15 — Dependence of the thermal diffusivity on annealing time for AZ91 with 22 vol% Saffil

were calculated from the electrical resistivity data. These values are lower than those given in [44]. We believe that this is a consequence of neglecting of the phonon thermal conductivity. The agreement between values estimated by steady state method [44] and non-steady state method (our data) is very good.

In order to give a reader an overview on the thermal conductivity of Mg alloys, the temperature variations of the thermal conductivities of some Mg alloys measured in our laboratory and presented in the literature are shown in Fig. 13.

### 3.2. Composites

The temperature dependence of the thermal diffusivity of the first, second and third runs for AZ91 with 22 vol% Saffil is shown in Fig. 14. The temperature dependencies for the second and third runs are almost the same and the values of the thermal diffusivity are higher than in the first run (similar behaviour as in the case of the unreinforced AZ91 alloy). Changes in the thermal diffusivity $\Delta a$ (measured at room temperature) between the first and the third run of the measurement for the solution treated (20°C) or isochronally annealed (140°C and 300°C) for reinforced and unreinforced AZ91 are presented in Tab. 3. It is supposed that precipitation in AZ91 matrix took place in the first run. Therefore, the values

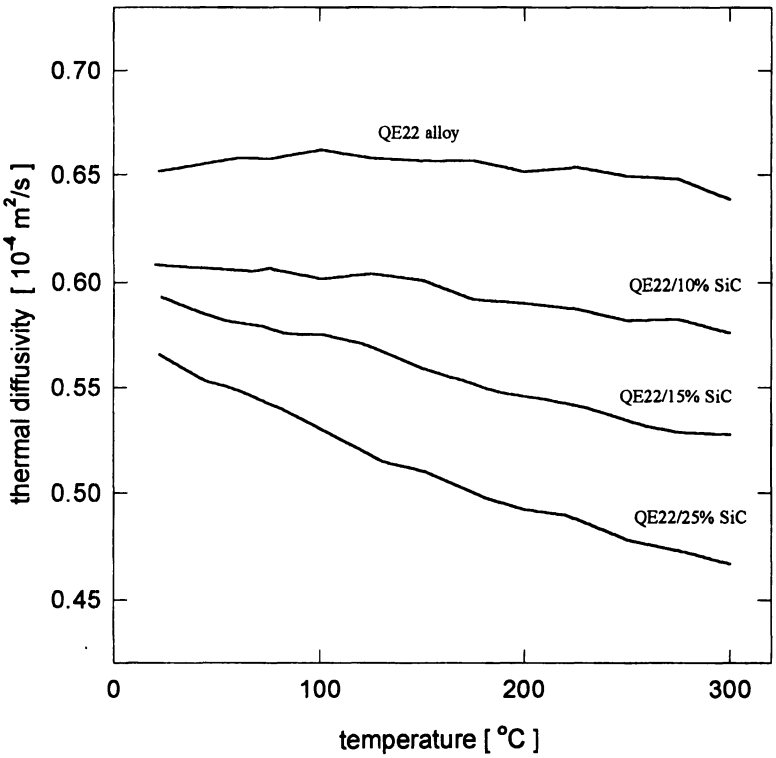


Fig. 16 — The temperature dependence of the thermal diffusivity of reinforced and unreinforced QE22 alloy

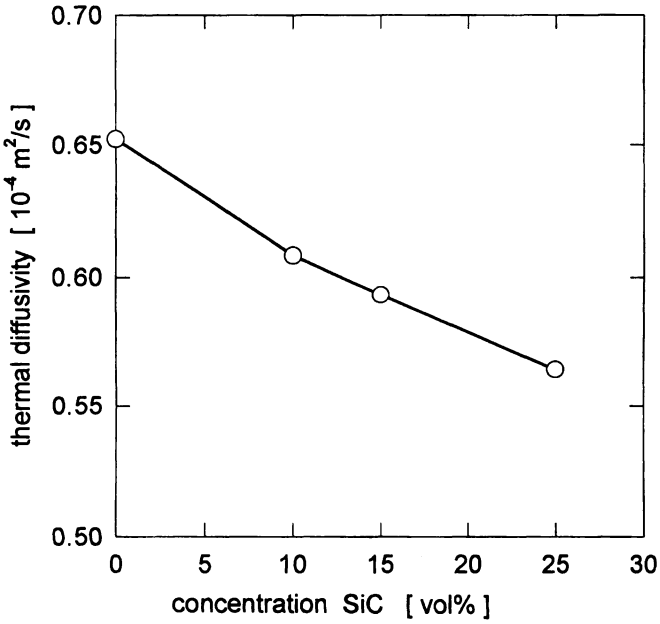


Fig. 17 — The concentration dependence of the thermal diffusivity of QE22/SiC composites

**Table 3** – Change of the thermal diffusivity $\Delta a$ between the first and the third run of the measurement for AZ91 specimens, solution treated (20°C) or isochronally annealed up to 140°C and 300°C, respectively.

| $\Delta a$ in % | upper temperature of isochronal annealing | | |
|---|---|---|---|
| $(a_{3,run} - a_{1,run})/a_{1,run}$ | 20°C | 140°C | 300°C |
| unreinforced | 8% | 9% | 3% |
| reinforced | 11% | 12% | 3% |

for the thermal diffusivity are lower at the beginning of the first run compared to the others runs. A preceding anneal at 300°C reduced $\Delta a$ value considerably due to accelerated precipitation in the temperature range from 200°C to 300°C. The difference $\Delta a$ for the reinforced specimens is slightly higher than that for the unreinforced alloy. This fact, which is in good agreement with electrical conductivity measurements [45], can be explained by the preferred precipitation of β-phase on the fibres due to heterogeneous nucleation and the Al enrichment of the matrix near

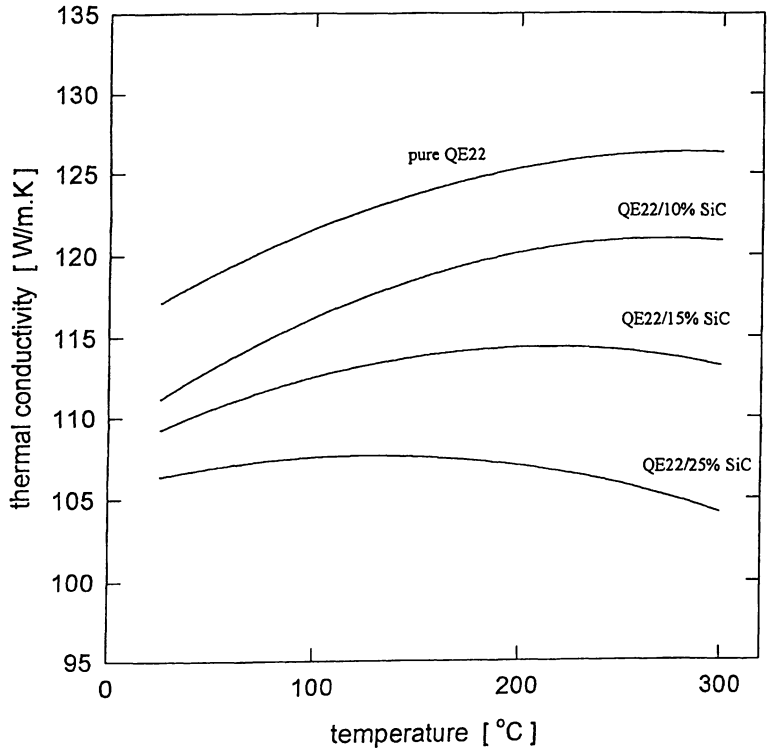


Fig. 18 – The temperature dependence of the thermal conductivity of reinforced and unreinforced QE22 alloy

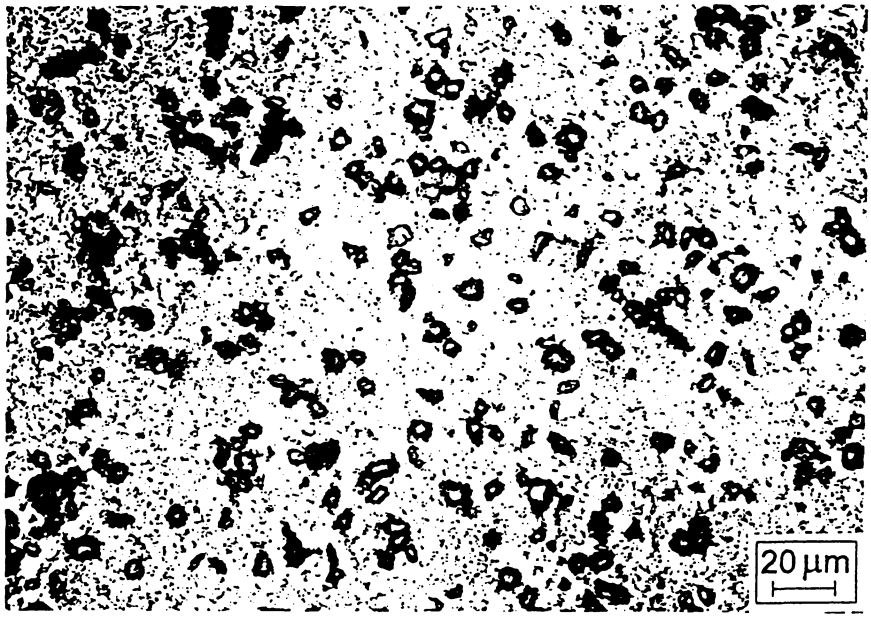


Fig. 19 – Optical micrograph of 15% SiC/QE22 composite

the alumina fibres. Heterogeneous nucleation of $Mg_{17}Al_{12}$ particles on grain boundaries in the AZ91 alloy has often been reported in the literature [9, 41, 42]. The influence of the precipitation on the thermal diffusivity of reinforced AZ91 is also mirrored by the influence of annealing time on *a* (Fig. 15). A reinforced AZ91 specimen was isochronally (20K/15min) annealed up to 100°C and then annealed for 3 hours at 150°C. The thermal diffusivity *a* of this specimen determined at this temperature is not influenced by the annealing time. After this measurement the specimen was subsequently cooled (1K/min) down to room temperature. The thermal diffusivity at 20°C was not affected by this procedure. A subsequent ageing treatment of the same specimen at 250°C for 2 hours raised the thermal diffusivity as shown in Fig. 15. The thermal diffusivity measured afterwards at 20°C had increased about 16%. Electrical resistivity as well as hardness measurements indicate a maximum for precipitation of solutes in the matrix at about 250°C [45, 46].

Mg alloy QE22 is also used for the preparation of composites. Figure 16 shows the temperature dependence of the thermal diffusivity for the QE22 alloy and three composites of QE22 matrix reinforced with SiC particles. From Fig. 16 it can be seen that whereas the thermal diffusivity of the unreinforced QE22 alloy is practically independent of temperature, the thermal diffusivity of composites decreases with increasing temperature. The drop in the thermal diffusivity depends on the volume fraction of SiC particles. The dependence of the

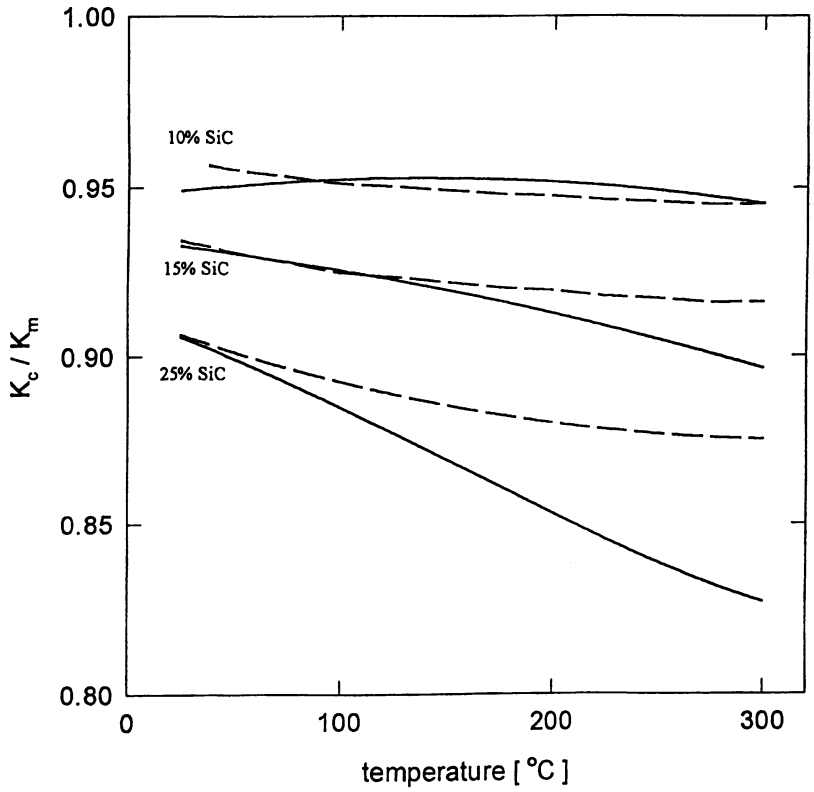


Fig. 20 — The temperature dependence of ratio $K_c/K_m$ (full lines — measured, broken lines — for $h$ = constant)

thermal diffusivity at room temperature on the SiC volume fraction is shown in Fig. 17.

The temperature dependencies of the thermal conductivity for the QE22 alloy and three composites are shown in Fig. 18. It can be seen that the thermal conductivity at any temperature decreases with increasing volume fraction of SiC particles. Whereas the temperature dependence of the thermal conductivity for the 10%SiC/QE22 composite is similar to that for the QE22 alloy, the temperature variation of the thermal conductivity for the composites with higher volume fractions of SiC particles is different from the former. The different thermal behaviour will be discussed in connection with the temperature dependence of the ratio $K_c/K_m$.

The ratio $K_c/K_m$ was calculated from the thermal conductivity of both components of the composite and the volume fraction of SiC particles considering the thermal conductance of the interface, $h$, (thermal conductance is inverse of the thermal boundary resistance) from the relation (16) deduced by Hasselman and Johnson [19] for composites with spherical particles

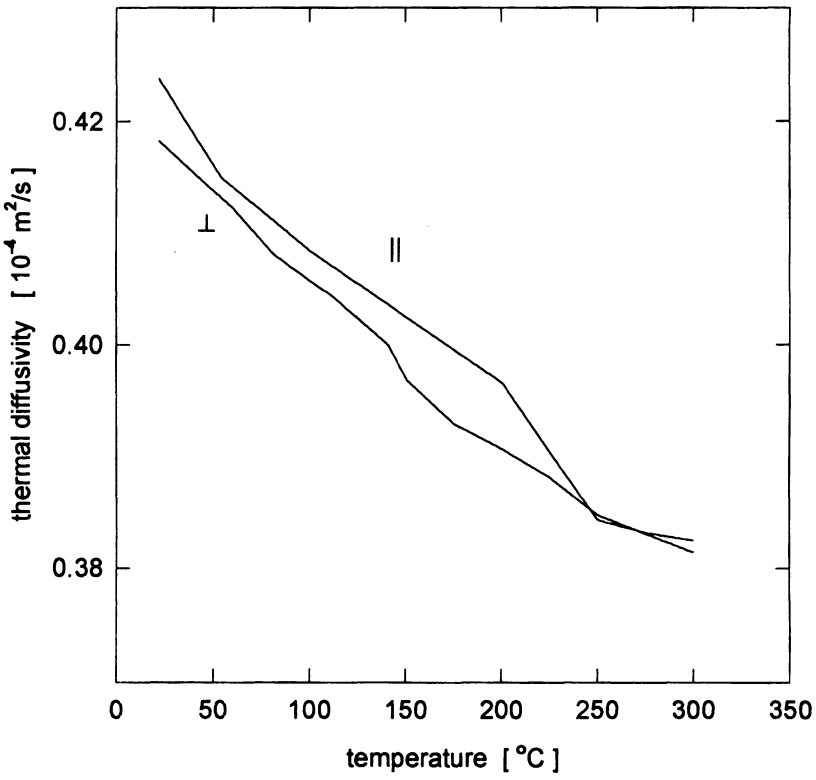


Fig. 21 – Temperature dependence of the thermal diffusivity of QE22/20 vol% Saffil composite

$$\frac{K_c}{K_m} = \frac{\left[2f\left(\frac{K_p}{K_m} - \frac{K_p}{r.h} - 1\right) + \frac{K_p}{K_m} + 2\frac{K_p}{r.h} + 2\right]}{\left[f\left(1 - \frac{K_p}{K_m} + \frac{K_p}{r.h}\right) + \frac{K_p}{K_m} + 2\frac{K_p}{r.h} + 2\right]} \tag{16}$$

where $K_p$ is the thermal conductivity of SiC particles and $r$ is their radius. The thermal conductivity of SiC decreases from $90\ W\ m^{-1}\ K^{-1}$ at room temperature at $80\ W\ m^{-1}\ K^{-1}$ at 300°C [47]. Fig. 19 shows the size, shape and distribution of particles in the SiC/QE22 composites used here. The temperature dependencies of the ratio $K_c/K_m$ experimentally measured and calculated are plotted in Fig. 20. The dashed curves were calculated according to equation (16) assuming that $h$ is constant. The value of $h$ is assumed to be, for all three composites, practically the same; (it varies between $7 \times 10^7$ and $1 \times 10^8\ W\ m^{-2}\ K^{-1}$). Comparing the results for the composites used here it is obvious that whereas there is good agreement between measured and calculated values of the thermal conductivity for the 10%SiC/QE22 composite in the whole range of temperature investigated here, there are some differences in these

values for the composites with higher volume fractions of SiC. For the 15%SiC/QE22 composite good correlation between calculated and measured value of the thermal conductivity is found for temperatures below 120°C. For the 25%SiC/QE22 composite the calculated and experimental data agree at room temperature only.

The electrical resistivity value of the QE22 alloy determined at 20°C is 66.5 nΩm [48]. The Lorenz number estimated from the thermal conductivity and electrical resistivity is about $2.65 \times 10^{-8}\,W\Omega K^{-2}$. This value provides evidence that the thermal conductivity of the QE22 alloy is predominantly via electrons. The scattering of electrons by lattice defects and phonons influences the electron thermal conductivity of the alloy. Three types of the lattice defects contributing to the scattering in the alloy matrix should be considered:

a) point defects such as foreign atoms;
b) dislocations in the matrix and in the vicinity of interfaces;
c) larger defects such as semicoherent precipitates and GP zones.

It has been shown by the acoustic emission and damping measurements [49] that when Mg composites are subjected to a temperature change without an applied

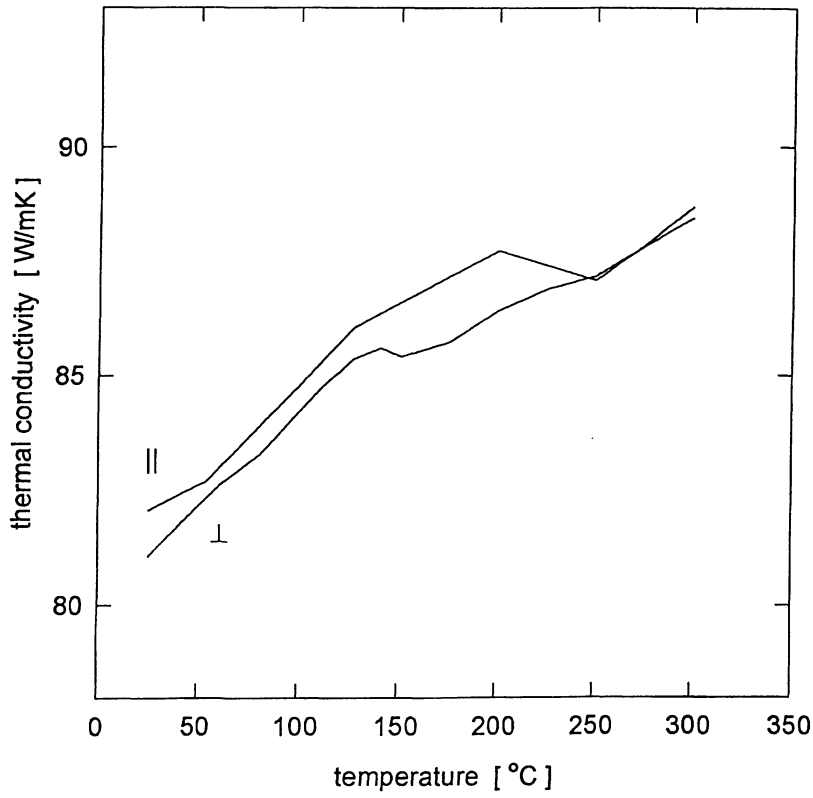


Fig. 22 – Temperature dependence of the thermal conductivity of QE22/20 vol% Saffil composite

stress, thermal stresses are induced in the matrix. The thermal stresses may relax by plastic deformation or diffusion processes [50]. The strain field, dislocations and other lattice defects increase the scattering of electrons and cause a decrease in the thermal conductivity of composite. The discrepancy between calculated and measured values of the ratio $K_c/K_m$ for 15%SiC/QE22 and 25%SiC/QE22 composite in Fig. 20 may be explained by decrease of the thermal conductivity of matrix in composite ($(K_m)_{com.} < (K_m)_{alloy}$) in surroundings of particles. The lattice defects are localized in the interface between particle and matrix at room temperature. During heating of composite the lattice defects expand into matrix and decrease its thermal conductivity. The largest decrease of the thermal conductivity in 25%SiC/QE22 composite is due to the highest concentration of particles and therefore the highest concentration of defects in this composite.

QE22 alloy was reinforced by 20 vol% Saffil fibres, too. The temperature dependence of the thermal diffusivity of this composite is shown in Fig. 21. The thermal diffusivity of composite with parallel orientation (∥) of fibres is higher than that for the composite with perpendicular (⊥) orientation of fibres up to

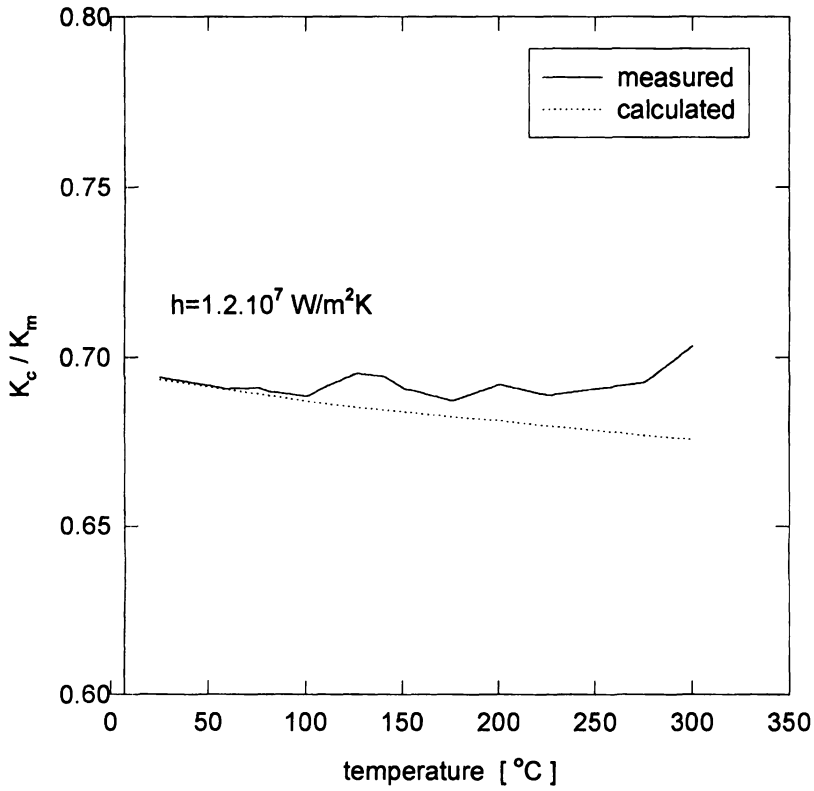


Fig. 23 – Temperature dependence of ratio $K_c/K_m$ for QE22/20 vol% Saffil ⊥ composite

250°C. Then there is no difference in the values of the thermal diffusivity for both composites. The temperature dependence of the thermal diffusivity for QE22/20 vol% Saffil ∥ can be divided into four ranges 1) up to 60°C, 2) between 60 and 200°C, 3) between 200 and 250°C and 4) between 250 and 300°C. The thermal diffusivity in ranges 1) and 3) decreases faster than in ranges 2) and 4).

The temperature dependencies of the thermal conductivity for the fibre composites are shown in Fig. 22. It can be seen that the thermal conductivity of the QE22/20 vol% Saffil ⊥ increases with increasing temperature in the whole temperature range. The thermal conductivity of the QE22/20 vol% Saffil ∥ composite increases with increasing temperature up to 200°C, then it decreases up to 250°C and at temperatures above 250°C it increases again and exhibits the same values as those for the composite with the perpendicular orientation.

The difference in the temperature variations of the thermal conductivity of QE22 composites with SiC particles and Saffil fibres may be treated by comparing of experimental values with those calculated according to Hasselman–Johnson models [19]. The relations (16) is for ratio of the thermal conductivity composite $K_c$ and thermal conductivity of matrix $K_m$ of particle composites. Hasselman and Johnson [19] derived a similar relation also for the fibre composite when the heat flow is perpendicular to fibres.

$$\frac{K_c}{K_m} = \frac{\left[f\left(\frac{K_f}{K_m} - \frac{K_f}{r.h} - 1\right) + \frac{K_f}{K_m} + \frac{K_f}{r.h} + 1\right]}{\left[f\left(1 - \frac{K_f}{K_m} + \frac{K_f}{r.h}\right) + \frac{K_f}{K_m} + \frac{K_f}{r.h} + 1\right]} \tag{17}$$

The thermal conductivity of Saffil decreases from 36 $W\,m^{-1}\,K^{-1}$ at room temperature to 17 $W\,m^{-1}\,K^{-1}$ at 300°C [47]. In Fig. 23 the experimental data are compared with the predictions derives from equation (17) for the fibre composite. Fig. 24 shows the size, shape and distribution of fibres in the QE22/20 vol% Saffil fibre composites. From the comparison of the particular and fibre composites it can be seen that while the experimental data for composites with particles are below calculated curve, the experimental data for the fibre composite are above calculated curve. The interface thermal conductance is $1.2 \times 10^7$ $W/m^2\,K$. The behaviour estimated for QE22/20 vol% Saffil ⊥ is very similar to that found for AZ91/22 vol% Saffil ⊥ composite [51]. Similar results have been reported for squeeze casting composite of Al/SiC [52].

## 4. Conclusions

The thermal diffusivity and thermal conductivity of Mg-Sc alloys increases with the temperature and decreases with the increasing concentration of Sc in Mg. The phonon thermal conductivity is nearly the same for all studied Mg-Sc alloys. The


Fig. 24 – Optical micrograph of QE22/20 vol% Saffil fibre composite; a) with parallel orientation of fibres to heat flow, b) with perpendicular orientation of fibres to heat flow

electronic thermal conductivity decreases from 160 W/m K for pure Mg up to 16 W/m K for Mg – 19.09 w%Sc alloy.

The thermal diffusivity of QE22 alloy is nearly the same in the temperature range from 20 to 300°C. The thermal conductivity of cp-Mg increases up to 100°C and further decreases. The thermal conductivity of QE22 and AZ91 alloys increases in the whole temperature range studied. The thermal diffusivity and thermal conductivity of AZ91 alloy are lower for the first run than those for further runs (where the values are the same). The differences between the first and further runs are due to precipitation which is connected with the purification of the alloy. The dependence of the thermal diffusivity on the precipitation processes (isochronally annealed up to various upper temperatures) shows a significant increase in the thermal diffusivity for isochronal annealing temperatures above 200°C. This is caused by removal of solutes from the alloy due to precipitation of the β-phase.

The thermal diffusivity and thermal conductivity of QE22 and AZ91 alloys reinforced by SiC particles and Saffil fibres was investigated and compared. The thermal diffusivity and thermal conductivity of QE22/SiC composites decrease with the increasing volume fraction of reinforcement and decrease with the increasing temperature. The largest decrease both parameters was found for the highest concentration of reinforcement. By comparison of the thermal conductivity of composites with the calculated values by the Hasselman – Johnson relation the thermal interface conductance was found about $1 \times 10^8$ W/m$^2$ K at room temperature. The departure of measured data from the calculated data for the highest concentration of SiC particles and the highest temperature is due to the highest concentration of lattice defects around particles. An anisotropic behaviour was found for the fibre QE22 composites. The different behaviour of QE22/20 vol% Saffil $\parallel$ and QE22/20 vol% Saffil $\perp$ is the most significant in the temperature range from 200°C to 250°C where the thermal diffusivity of the first composite decreases while for QE22/20 vol% Saffil $\perp$ increases. The interface thermal conductance of this composite is $1.2 \times 10^7$ W/m$^2$ K. This value is lower than that for QE22 particle composite.

## Acknowledgements

The authors appreciate support from the Grant Agency of the Czech Republic under grant 106/99/1717 and the Grant Agency of the Academy of Sciences under the grant A2041902.

## References

[1] KINGERY W. D., Property measurements at high temperatures, John Wiley & Sons, Inc., New York (1959).

[2] CHARVAT F. R., KINGERY W. D., J. Amer. Ceram. Soc. **40**, 306, (1957).

[3] CARSLAW F. R., JAEGER J. C., Conduction of heat in solids 2nd ed. Oxford Univ. Press London (1959).

[4] KR. AUNE T., WESTENGEN H., International Congress and Exposition. Detroit, Michigan 1995, p. 21.
[5] BERMAN R., Thermal conduction in solids, Clarendon Press Oxford 1976.
[6] HÖLRIGL-ROSTA F., JUST E., KÖHLER J., MELZER H. J. in Proc. '37th Annual World Magnesium Conference' 38; International Magnesium Association, Dayton OH, 1980.
[7] WALTRIP J. S., in Proc. '47th Annual World Magnesium Conference' 124; International Magnesium Association, 1990, Mc Lean, VA.
[8] KING J. F., Advanced materials technology international, (ed. G. B. Brook), Vol. 12, Sterling London, 1990
[9] POLMEAR I. J., Mat. Sci. Technol. **10**, 1, (1994).
[10] KELLY A., Phil. Trans. Mag. **34**, 481, (1987).
[11] HASNEH C. H., BECHER P. F., J. Mat. Sci. Lett. **10**, 1165, (1991).
[12] HASSELMAN D. P. H., J. Comp. Mat. **12**, 9 (1978).
[13] XU, Z. R., CHAWLA K. K., WOLFEDEN A., NEUMAN A., LIGGETT G. M., CHAWLA N., Mat. Sci. Eng. A **203**, 75, (1995).
[14] FLORENCE A. L., GOODIER J. N., Appl. Mech. **26**, 293, (1959).
[15] FLORENCE A. L., GOODIER J. N., Appl. Mech. **27**, 6359, (1960).
[16] FLORENCE A. L., GOODIER J. N., Int. J. Engng. Sci. **1**, 533, (1963).
[17] TAUCHER T. R., J. Comp. Mat. **2**, 478, (1968).
[18] P. L. KAPITZA, Collected Papers of P. L. Kapitza, ed. D. ter Haar, Vol. 2, p. 581, Pergamon Press, Oxford (1965).
[19] HASSELMAN D. P. H., JOHNSON L. F., J. Comp. Mater. **21**, 508, (1987).
[20] KRUPIECZKA R., Int. Chem. Eng. **7**, 122, (1967).
[21] CRANE R. A., VACHON R. I., Int. Heat Mass Transfer **20**, 711, (1976).
[22] OCHIAI S., Mechanical properties of metallic composites, Marcel Dekker, Inc. New York, Basel, Hong Kong 1994.
[23] PARKER W. J., JENKINS R. J., BUTLER C. P., ABBOT G. L., J. Appl. Phys. **32**, 1679, (1961).
[24] KERRISK J. F., J. Appl. Phys. **42**, 267, (1971).
[24] KERRISK J. F., J. Appl. Phys. **43**, 112, (1971).
[26] MORDIKE B. L., KAINER K. U., MOLL F., SOMMER B., Proceedings of the First Israeli International Conference of Magnesium Science & Technology. Dead Sea, Israel 1997, p. 178.
[27] MOLL F., KAINER B. L., MORDIKE B. L. in: Magnesium Alloys and their Applications. Ed. B. L. Mordike, K. U. Kainer, Werkstoff-Informationsgesellschaft, Frankfurt 1998 (p. 647).
[28] ZHENG M., WU K., ZHAO M., YAO C., LI J., LI D., J. Mat. Sci. Lett. **16**, 1106, (1997).
[29] KIEHN J., KOHLER C., KAINER K. U., Key Engng. Mat. **97–98**, 37, (1994).
[30] KIEHN J., SMOLA B., VOSTRÝ P., STULIKOVÁ I., KAINER K. U., Phys. Stat. Sol. (a) **164**, 709, (1997).
[31] DODD S. B., MORRIS S., WARDINER R. W., Proceedings of the First Israeli International Conference on Magnesium Science & Technology, Dead Sea, Israel 1997, p. 337.
[32] CAPE J. A., LEHMAN G. W., J. Appl. Phys. **14**, 1909, (1963).
[33] WALTER A. J., GILCHRIST K. E., TAYLOR R., High Temp.-High Press. **4**, 439, (1972).
[34] LIU D., J. Mat. Sci., **31**, 86, (1996).
[35] RUDAJEVOVÁ A., Mater. Res. Bull. **26**, 1363, (1991).
[36] RUDAJEVOVÁ A., KIEHN J., KAINER K. U., MORDIKE B. L., LUKÁČ P., Scripta Mater. **40**, 57, (1999).
[37] NORDHEIM L., Ann. Phys. **9**, 6007, (1931).
[38] TERADA Y., NAKATA J., MOHRI T., SUZUKI T., Intermetallics **6**, 479, (1998).
[39] VOSTRÝ P., STULIKOVÁ I., SMOLA B., VON BUCH F., MORDIKE B. L., Proceedings of the First Israeli International Conference on Magnesium Science & Technology. Dead Sea, Israel 1997, p. 88.

[40] BETTLES C. J., HUMBLE P., NIE J. F., Proceedings of the 3rd International Magnesium Conference, ed. G. W. Lorimer p. 403, The Institute of Materials, London (1997).

[41] POLMEAR I. J., Magnesium Alloys and Their Applications, ed. B. L. Mordike and F. Hehmann, p. 201, DGM, Oberursel (1992).

[42] COLLETO S., BASTOW T. J., HUMBLE P., BETLLES C. J., Proceedings of the 3rd International Magnesium Conference, ed. G. W. Lorimer p. 391, The Institute of Materials, London (1997).

[43] NHMg. db. Hydro Magnesium, Norsk Hydro a.s. 1996.

[44] KASCHNITZ E., FUNK W., Geißerei-Praxis **7/8**, 179, (1997).

[45] KIEHN J., KAINER K. U., VOSTRY P., STULIKOVÁ I., Phys. Stat. Solidi **161**, 85, (1997).

[46] BUCHHAGEN P., RIEHEMANN W., MORDIKE B. L., Magnesium Alloys and Their Applications, ed. B. L. Mordike and F. Hehmann, p. 229, DGM, Oberursel (1992).

[47] Handbook of Chemistry and Physics, ed. D. R. Lide, 73rd edition, 1992 – 1993.

[48] KIEHN J., KAINER K. U., VOSTRÝ P., STULIKOVÁ I., phys. stat. sol. (a) **164,** 709, (1997).

[49] LUKÁČ P., TROJANOVÁ Z., CHMELÍK F., KIEHN J., Inzynieria Materialowa **50**, 130, (1998).

[50] SINCLAIR I., GREGSON P. J., Mat. Sci. Technol. **13**, 709, (1997).

[51] RUDAJEVOVÁ A., KIEHN J., LUKÁČ P., KAINER K. U., MORDIKE B. L. in: Magnesium Alloys and their Applications. Ed. B. L. Moírdike, K. U. Keiner, Werkstoff-Informationsgesellschaft, Frankfurt 1998 (p. 665).

[52] ELOMARI S., BOUKHILI R., LLOYD D. J., J. Mat. Sci. **32**, 2131, (1997).